First-principles study on interlayer states at the 4H-SiC/SiO_2 interface and the effect of oxygen-related defects

Christopher James Kirkham[1 *] and Tomoya Ono[1,2 †]

[1]*Center for Computational Sciences, University of Tsukuba, Tsukuba, Ibaraki 305-8577, Japan*

[2]*JST-PRESTO, Kawaguchi, Saitama 332-0012, Japan*

We investigate the effect of SiC stacking and interfacial O defects on the electronic structure of the 4H-SiC/SiO_2 interface via first-principles calculations. We find interlayer states along the SiC conduction band edge, whose location changes depending on which of two possible lattice sites, *h* or *k*, is at the interface. Excess O atoms at the interface lead to defect structures which alter the electronic structure. Changes to the valence band edge are the same whether *h* or *k* sites are at the interface. On the other hand, defects remove the interlayer state of the conduction band edge between the first and second SiC bilayers if an *h* site is at the interface, but have no effect when there is a *k* site. The variation of the conduction band edge at the interface is interpreted in terms of floating states, a particular property of SiC.

1. Introduction

Silicon carbide (SiC) is a wide band-gap semiconductor material with the potential to replace Si for high temperature and power electronic devices. Like Si, its native oxide is SiO_2, which can be grown via thermal oxidation, making it useful for metal-oxide-semiconductor field-effect transistors (MOSFETs), primarily of the n-channel type. However, its use in practical devices has been hampered by the low channel mobility of the SiC/SiO_2 interface compared with bulk SiC.[1,2] Interfacial defects[3–6] have attracted a lot of attention, with the aim of identifying and removing the most detrimental. Traditionally, research has focused on defects which contribute interface gap states, but advances in interface growth techniques mean that these gap states no longer make a significant contribution to reductions in mobility.[7–9] Despite this, mobility still lags behind the ideal value, meaning that further improvements will require new information.

*kirkham@ccs.tsukuba.ac.jp
†ono@ccs.tsukuba.ac.jp

SiC has many different polytypes, determined based on their stacking along the [0001] direction. Si and C atoms can occupy one of three positions along the $[1\bar{1}00]$ direction, normally labelled ABC. Stacking ordered ABCAB... is called cubic whilst that ordered ABABA... is called hexagonal. Polytype is determined by the shortest repeated unit of these positions in the [0001] direction. The most commonly used polytype for electronic devices is 4H-SiC, which consists of four repeated SiC bilayers, ordered ABCBAB..., as shown in Fig. 1. Within these four bilayers, there are two inequivalent lattice sites, usually known as *h* (hexagonal) and *k* (quasi-cubic) based on the site occupied by the Si atoms in the neighboring bilayers. *h* sites are equivalent to A or C stacking positions and *k* sites are equivalent to B stacking positions. The local structure around the SiC/SiO_2 interface will change depending on which of these stackings is at the SiC surface.[10,11] For convenience, we refer to the surfaces which end at A or C stacking positions as *h* type and those ending at B stacking positions as *k* type following the definition proposed in Ref. 12.

It is reported that *floating* states, whose charge density accumulates in the interlayer region, rather than near atomic sites, lie near the conduction band edge (CBE) in elemental semiconductors.[13] Previous work looking at bulk SiC found that interlayer floating states appear between subsequent SiC bilayers with cubic stacking, and lie at the CBE.[13] A subsequent study of superlattice structures consisting of hexagonal and cubic stacking regions revealed that the floating states at the CBE accumulate within the cubic stacking region due to the spontaneous polarization induced by differences in electronegativity between Si and C.[14] It is of interest how the floating states behave at the SiC/SiO_2 interface because the electronegativity of O is much larger than C and SiC/SiO_2 interfaces are generally used for practical MOSFETs.

Theoretical studies report that C and O-related defects[15] are created during the thermal oxidation process.[3,4,6] Of these, the density of C-related defects is measurable since they generate gap states. Recent experimental studies have reported that the density of defects which generate these states is less than 10^{-12} cm^{-2} eV^{-1}.[16] On the other hand, O defects constitute necessary steps of the oxidation process, so are expected to be found in higher densities. Here we investigate how the local density of states (LDOS) of the SiC/SiO_2 interface changes depending on the stacking of SiC bilayers at the interface, i.e. *h* and *k* types, and when O defects are subsequently introduced. Currently the stacking of the SiC substrate at the oxidation front cannot be controlled during the thermal oxidation process, so both interface types exist in practical devices. Due to differences in local structure, CBE floating states are observed from the first SiC bilayer for *h* type, but from the second bilayer for *k* type. More interestingly,

defects behave differently in h and k type, removing the floating states at the h type whilst leaving the k type unchanged. This characteristic behavior of the LDOS is explained by the nature of the floating states, and will affect the performance of present SiC-MOSFETs, which rely on the electronic structure at the CBE.

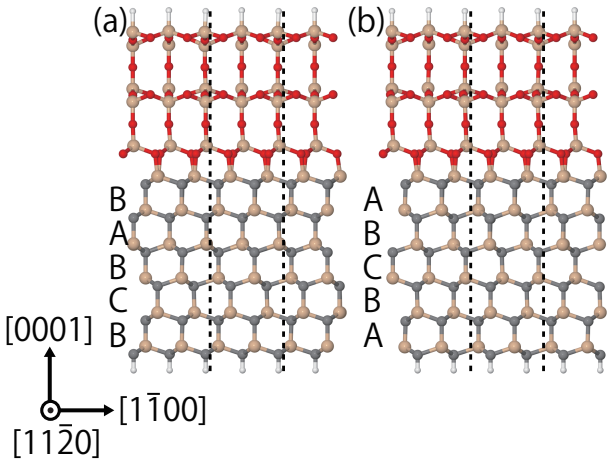

Fig. 1. (Color online) SiC/SiO_2 interface with (a) h and (b) k lattice sites at the interface. Dashed lines indicate the bounding box of the calculation supercell. Si atoms are beige, C grey, O red and H white.

2. Methods

Calculations are carried out using RSPACE,[17] which performs density functional theory[18,19] calculations using a real-space finite-difference method,[20] employing a time-saving double-grid technique.[21–23] The electron-ion interactions are described using the projector-augmented wave method[24] for the C, Si and O atoms, and a norm-conserving pseudopotential[25,26] for H. The exchange-correlation interaction is treated within the local density approximation.[27]

The interface is modelled using 6 bilayers of 4H-SiC and 9 Å thick of β-tridymite SiO_2, with the interface made at the SiC(0001) surface, saturating all the Si dangling bonds with O. Both the top and bottom layers of the model are H terminated. The interface is constructed using experimental values for the Si-C and Si-O bond lengths. The lateral size of the cell is SiC(0001) $3 \times \sqrt{3}$ with the z direction perpendicular to the SiC surface. The cell is periodic in all directions with an 11 Å vacuum gap in the z direction. Calculations are performed with a coarse grid spacing of 0.16 Å and using the Γ and M k-points of SiC(0001) $3 \times \sqrt{3}$. The bottom H atoms and SiC bilayer are held fixed and structural optimization is performed on all remaining atoms to reduce the forces between atoms. A variety of known defects[3–6] are

introduced into the SiC. Full details on interface atomic structures including defects will be described later.

We examine the LDOS for both types of interface, with and without defects. The LDOS is calculated according to

$$\rho(z, E) = \sum_{i,k} \int |\Psi_{i,k}(x, y, z)|^2 \mathrm{d}x\mathrm{d}y \times N e^{-\alpha(E-\varepsilon_{i,k})^2} \tag{1}$$

where $\varepsilon_{i,k}$ are the eigenvalues of the wavefunction, with indexes of i and k for the eigenstate and the k-point respectively. $N = 2\sqrt{\frac{\pi}{\alpha}}$ is the normalisation factor, with α as the smearing factor, here set to 13.5 eV^{-2}.

3. Results and Discussion

As mentioned earlier, there are two types of clean interface in 4H-SiC(0001), depending on whether an h or k site is at the interface. Before considering defects it is useful to see how these differ. We find that the difference in the total energy between the h type and k type is less than 1 meV per 1×1 region when the contribution from the bottom SiC surface is subtracted. This energy difference is much smaller than is observed for surfaces (32.4 meV).[28] This suggests that both the h and k types appear at the oxidation front, whilst the h type is dominant in the case of surfaces.[10,11] Figure 2 shows the LDOS for the h and k types. There are no significant changes at the valence band edge (VBE) of the SiC substrate. On the other hand, the most interesting results are along the CBE, where several yellow oval-like features are observed, the location of which changes with interface type. The h type has one of these oval-like features at the first bilayer of the interface, whereas one does not appear until the second bilayer for the k type. The states which contribute to the oval-like features at the CBE are the previously noted floating states,[13,14] which only appear at the CBE in the cubic stacking regions (ABC or CBA) and are blocked by the hexagonal stacking regions. The charge density of the floating states accumulates within the cubic stacking region, as shown in Fig. 3 for the h type. The first two bilayers of the h type correspond to cubic stacking, compared to the second and third bilayers of the k type, explaining why the first floating state is observed further from the interface in the k type. As a result, the interfacial band gap changes with interface type. It is reported that the charge density of the CBE in a superlattice structure consisting of 2H and 3C distributes near one of the interfaces between lattice types, therefore the center of the density of the floating state shifts upward.[29]

To aid with future discussions on this matter, we introduce channel length, a measure of

the length of subsequent SiC bilayers with cubic stacking.[14] A minimum channel length of three is required to observe floating states. The longest channel length for bulk 4H-SiC is three. Just below the first interface bilayer of the *h* type, the channel length is also three, but the length is only two in *k* type.

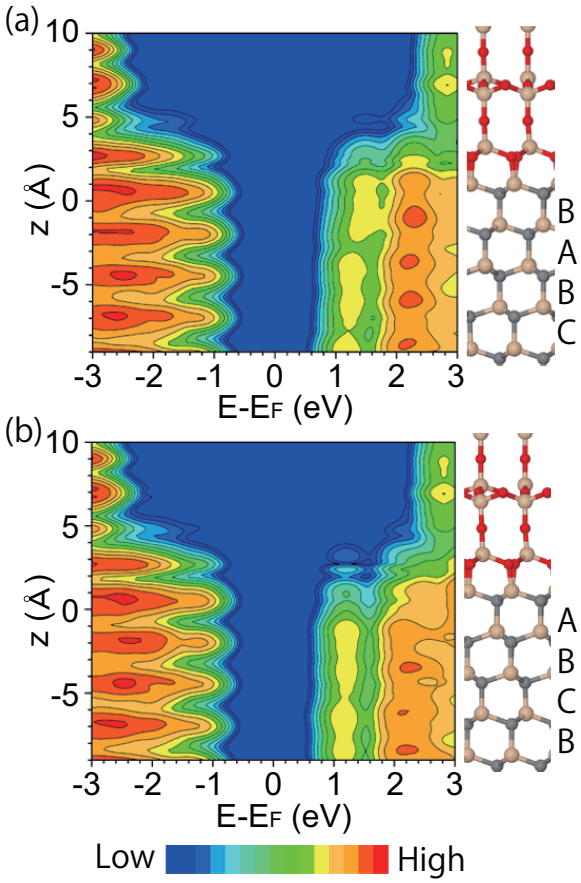

Fig. 2. (Color online) LDOS for the clean (a) *h* and (b) *k* types. The horizontal axis is energy relative to the Fermi energy, E_F, defined as the middle of the band gap. The vertical axis is the height of the model. For clarity, structural models are provided to the right of each LDOS. Contours correspond to density, from blue at the lowest to red at the highest, doubling at each contour line, from a minimum of 5.3×10^{-7} states $eV^{-1}Å^{-1}$.

It is interesting to consider the influence of O defects, which are introduced during thermal oxidation, since they exist within or just below the first SiC bilayer; the region where the interface types differ. We focus on the most stable defects identified in our previous study[6] for each stage of one oxidation cycle. Structures for each are shown in Fig. 4. For the initial step, involving one O defect, the most stable structure is O_{if}[3] [Fig. 4(a)], an interstitial site at the interface. For the next step, involving two O defects, O_{sub}+O_{if}[5] [Fig. 4(b)] is the most stable, combining an interstitial and subsurface site. The final step is V_CO_2[4] [Fig. 4(c)], which

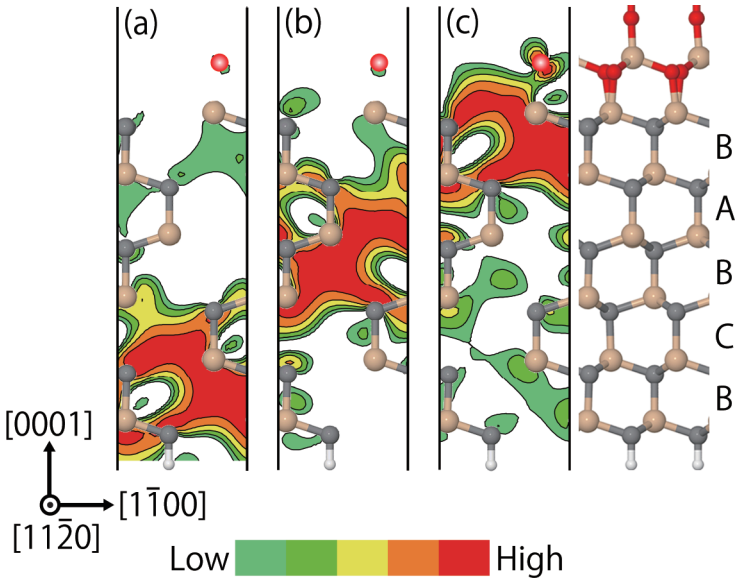

Fig. 3. (Color online) Charge density distribution for the three lowest energy CBE states of the *h* type interface, showing floating states between the (a) fifth and sixth, (b) third and fourth, and (c) first and second bilayers. Charge densities are shown through a plane down the center of the computational model. To clarify the position of the interface a full structural model is provided to the right. Contours correspond to density, from light green at the lowest to red at the highest, doubling at each contour line, from a minimum of 4.2×10^{-6} states $eV^{-1}Å^{-1}$.

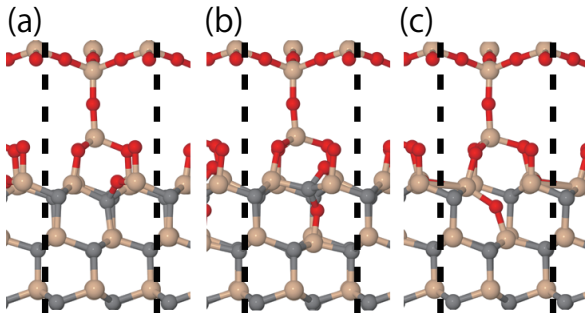

Fig. 4. (Color online) Structural models for various O defects in the *h* type. (a) O_{if}. (b) O_{sub}+O_{if}. (c) V_CO_2. All are shown looking down the [11$\bar{2}$0] direction. Dashed lines indicate the bounding box of the calculation supercell.

appears after introducing three excess O atoms and removing a CO molecule to relieve the interface stress caused by lattice constant mismatch.

We examine the LDOS for each structure, noting how it changes compared to the clean interfaces. We start with one O defect, as shown in Figs. 5 (a) and (b). Notably, the CBE of the *h* type changes, whilst that of the *k* type does not. In bulk SiC, a C atom takes electrons from the surrounding Si atoms, resulting in lower electrostatic potential at the Si-surrounded tetrahedral interstitial site than that at the C-surrounded site.[13] Due to the low electrostatic

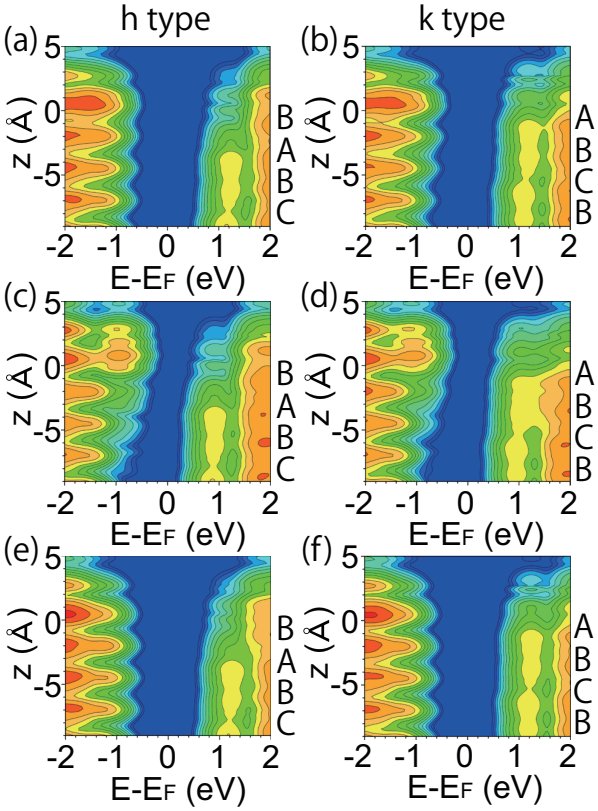

Fig. 5. (Color online) LDOS for a variety of defects in both the *h* and *k* types, with each pair presented in that order. (a)-(b) O_{if}. (c)-(d) O_{sub}+O_{if}. (e)-(f) V_CO_2. Notation is the same as Fig. 2. These LDOS focus on the region around the SiC band gap and SiC/SiO_2 interface from Fig. 2.

potential at the Si-surrounded site as well as the broad orbital distribution in the ⟨110⟩ channel direction of cubic stacking, the floating states appear in the cubic stacking region. In the *h* type case, an O atom is inserted into one of the Si–C bonds forming a Si-surrounded tetrahedron in which the floating states are formed. Since O is strongly electronegative, the electrostatic potential at the Si-surrounded site is no longer low, and the first floating state is shifted upwards in energy, increasing the band gap. On the other hand, the *k* type shows no significant changes at the CBE because there is no floating state to influence. Changes at the VBE are the same across interface types. The VBE around the defect location shifts upwards in energy slightly. This defect state can be attributed to a C–O π bond, as observed in the partial DOS for the highest occupied band (not presented here). Because the dissociation energy of a C–O bond at the SiC/SiO_2 interface is lower than that of a Si–C bond,[30] the VBE at the interface shifts up in energy slightly, but the defect state is indistinct from the bulk SiC states.

Next we examine two O defects, as shown in Figs. 5 (c) and (d). The same changes are observed at the CBE as before, with the interface floating state removed for *h* type. Although

the second O atom exists between the first and second bilayers, there are no notable changes to the CBE deep within the SiC substrate because the next Si-surrounded tetrahedron in which the floating states appear is formed between the third and fourth SiC bilayers. In the *k* type case, the Si-surrounded tetrahedron formed between the second and third bilayers is also preserved, therefore the LDOS at the CBE is unaffected. On the other hand, a defect state seen at the VBE is more distinct from the bulk SiC than for one O defect. Examining the partial DOS for the highest occupied bands shows that this defect state again arises from C–O π bonds. Since O_{sub}+O_{if} contains an O–C–O bond, the defect states associated with C–O π bonds are even higher in energy, making them distinct from the VBE.

Finally, we consider the V_CO_2 structure, which looks similar to the clean interface. Figs. 5 (e) and (f) shows the LDOS of V_CO_2 structure. Although one CO molecule is removed from the vicinity of the Si-surrounded tetrahedron, there still remains two O atoms. Therefore the floating states do not recover for the *h* type. For the *k* type, the CBE is not changed because the tetrahedron is located deep inside the substrate. In addition, no changes are observed at the VBE for both types, because there are no C–O bonds in the V_CO_2 structure.

These results are summarized, using band diagrams instead of LDOS, in Figs. 6 and 7 for the *h* and *k* types, respectively. For the clean *h* type interface, shown in Fig. 6 (a), the band gap is approximately the same throughout the SiC. When defects are introduced, the band diagram is modified. For the *h* type, states at the CBE are removed, opening the band gap near the interface. The expanded band gap extends down to the second bilayer because the state that would appear there is removed. For the *k* type, states attributed to the floating states are not observed at the interface, as shown in Fig. 7, whether defects are present or not. The extent of the gap is approximately half that of the *h* type, because it only corresponds to the first SiC bilayer. On the VBE side, a defect state formed by C–O bond can appear near the VBE for O_{if} and O_{sub}+O_{if} in both the *h* and *k* type cases.

To make sure that the behavior at the CBE reported above is not exclusive to O, we investigated C-related defects, such as C and C_2 interstitials, which have been reported at the SiC/SiO_2 interface in prior work.[3,4] Changes at the CBE are partially obscured by a defect state close to the CBE introduced by C. However, we still observe that the floating states of the *h* type are easily affected by the defects, whilst the *k* type is insensitive to their presence. Changes are observed for *h* type because the inserted C and C_2 raise the electrostatic potential in the tetrahedron.

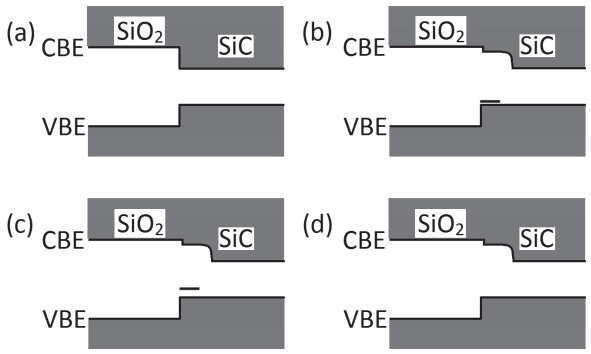

Fig. 6. Schematic band diagrams for the *h* type SiC/SiO_2 interface, highlighting important changes caused by defects. (a) Clean interface. (b) O_{if}. (c) O_{sub}+O_{if}. (d) V_CO_2.

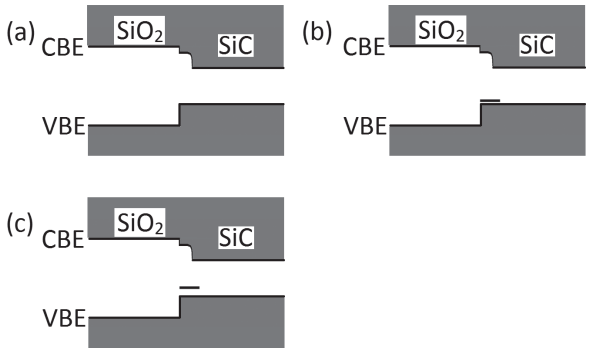

Fig. 7. Schematic band diagrams for the *k* type SiC/SiO_2 interface, highlighting important changes caused by defects. (a) Clean interface and V_CO_2. (b) O_{if}. (c) O_{sub}+O_{if}.

4. Conclusions

We have carried out first-principles calculations on the relationship between the interface type of SiC/SiO_2 and its LDOS. It is found that interface type determines whether CBE floating states at the interface are affected by the presence of O defects, as with *h* type, or not, as with *k* type. Floating states are observed between adjacent SiC bilayers within the cubic stacking region and are found from the first bilayer down for the *h* type interface and from the second bilayer down for the *k* type. When O defects are introduced at the interface, the inserted O atoms raise the electrostatic potential of the Si-surrounded tetrahedral interstitial site due to the strong electronegativity of O, removing the floating state at the *h* type interface. In the *k* type case, changes at the CBE are negligible since there are no states to remove. On the other hand, although defect states are found at the VBE, arising from the C–O π bonds formed by the O defects, there are no significant differences in the LDOS between the *h* and *k* types. Since recent SiC-based MOSFETs mainly use the conduction band as a channel, the

behavior of these floating states might play an important role in the performance of these devices. In the future we want to do more complete calculations for all of these structures, to get a fuller picture of how the scattering properties of the interface change with defect type using first-principles transport calculations.

Acknowledgements

This work was supported by the Computational Materials Science Initiative (CMSI). The numerical calculations were carried out using the computer facilities of the Institute for Solid State Physics at the University of Tokyo.

References

1) VV. Afanas'ev, M. Bassler, G. Pensl, and M. Schulz, Phys. Status Solidi A **162**, 321 (1997).

2) VV. Afanas'ev, F. Ciobanu, S. Dimitrijev, G. Pensl, and A. Stesmans, J. Phys.: Condens. Matter **16**, S1839 (2004).

3) J. Knaup, P. Deák, T. Frauenheim, A. Gali, and Z. Hajnal, and W. J. Choyke, Phys. Rev. B **71**, 235321, (2005).

4) P. Deák, J. Knaup, T. Hornos, C. Thill, A. Gali, and T. Frauenheim, J. Phys. D **40**, 6242 (2007).

5) A. Gavrikov, A. Knizhnik, A. Safonov, A. Scherbinin, A. Bagatur'yants, and B. Potapkin, A. Chatterjee, and K. Matocha, J. Appl. Phys. **104**, 093508 (2008).

6) T. Ono and S. Saito, Appl. Phys. Lett. **106**, 081601 (2015).

7) S. Dhar, S. Haney, L. Cheng, S.-R. Ryu, A. K. Agarwal, L. C. Yu, and K. P. Cheung, J. Appl. Phys. **108**, 054509 (2010).

8) P. Fiorenza, F. Giannazzo, M. Vivona, A. La Magna, and F. Roccaforte, Appl. Phys. Lett. **103**, 153508 (2013).

9) G. Liu, B.R. Tuttle, and S. Dhar, Appl. Phys. Rev. **2**, 021307 (2015).

10) K. Arima, H. Hara, J. Murata, T. Ishida, R. Okamoto, K. Yagi, Y. Sano, H. Mimura, and K. Yamauchi, Appl. Phys. Lett. **90**, 202106 (2007).

11) K. Arima, K. Endo, K. Yamauchi, K. Hirose, T. Ono, and Y. Sano, J. Phys.: Condens. Matter **23**, 394202 (2011).

12) W. Suttrop, G. Pensl, W. J. Choyke, R. Stein and S. Leibenzeder, J. Appl. Phys. **72**, 3708 (1992).

13) Y. Matsushita, S. Furuya, and A. Oshiyama, Phys. Rev. Lett. **108**, 246404 (2012).

14) Y. Matsushita and A. Oshiyama, Phys. Rev. Lett. **112**, 136403 (2014).

15) The term O defects is used to indicate O interstitials and C vacancies passivated with two excess O atoms. Since these structures do not generate clear gap states, it might be inadequate to refer to them as O defects. However, we refer to these structure as O defects following Refs. 3 and 4.

16) D. Okamoto, H. Yano, K. Hirata, T. Hatayama and T. Fuyuki, IEEE Electron Device Lett. **31**, 710 (2010).

17) K. Hirose, T. Ono, Y. Fujimoto, and S. Tsukamoto, *First Principles Calculations in Real-Space Formalism, Electronic Configurations and Transport Properties of Nanostructures* (Imperial College, London, 2005).

18) P. Hohenberg and W. Kohn, Phys. Rev. **136**, B864 (1964).

19) W. Kohn and L. J. Sham, Phys. Rev. **140**, A1133 (1965).

20) J. R. Chelikowsky, N. Troullier, and Y. Saad, Phys. Rev. Lett. **72**, 1240 (1994).

21) T. Ono and K. Hirose, Phys. Rev. Lett. **82**, 5016 (1999).

22) T. Ono and K. Hirose, Phys. Rev. B **72**, 085115 (2005).

23) T. Ono, M. Heide, N. Atodiresei, P. Baumeister, S. Tsukamoto, and S. Blügel, Phys. Rev. B **82**, 205115 (2010).

24) P.E. Blöchl, Phys. Rev. B **50**, 17953 (1994).

25) L. Kleinman and D.M. Bylander, Phys. Rev. Lett. **48**, 1425 (1982).

26) N. Troullier and J.L. Martins, Phys. Rev. B **43**, 1993 (1991).

27) S. H. Vosko, L. Wilk, and M. Nusair, Can. J. Phys. **58**, 1200 (1980).

28) H. Hara, Y. Morikawa, Y. Sano, and K. Yamauchi, Phys. Rev. B **79**, 153306 (2009).

29) Y. Sugihara, K. Uchida, and A. Oshiyama, J. Phys. Soc. Jpn. **84**, 084709 (2015).

30) T. Akiyama, A. Ito, K. Nakamura, T. Ito, H. Kageshima, M. Uematsu, K. Shiraishi, Surf. Sci. **641**, 174 (2015).